Network-Coded Multiple Access with Higher-order Modulations

Haoyuan Pan*, Lu Lu† and Soung Chang Liew*
*Department of Information Engineering, The Chinese University of Hong Kong, Hong Kong.
†Institute of Network Coding, The Chinese University of Hong Kong, Hong Kong.
Email:{ph014, lulu, soung}@ie.cuhk.edu.hk

arXiv:1504.03426v1 [cs.IT] 14 Apr 2015

***Abstract*—This paper presents the first network-coded multiple access (NCMA) system operated on higher-order modulations beyond BPSK. NCMA allows multiple nodes to transmit simultaneously to an access point (AP) to boost throughput of wireless local area networks (WLAN): the key idea is to jointly exploit multiuser decoding (MUD) and physical-layer network coding (PNC). High-order modulations are commonly adopted in WLAN systems when the signal-to-noise ratio (SNR) is medium or high. However, direct generalization of the existing NCMA decoding algorithm, originally designed for BPSK, to higher-order modulations will lead to huge performance degradation. We find that the throughput degradation is caused by the relative phase offset between received signals from different nodes. To circumvent the throughput degradation, this paper investigates an NCMA system with multiple receive antennas at the AP, referred to as MIMO-NCMA. We have implemented MIMO-NCMA on software-defined radios. Our experimental results show that, at SNR of 10dB, the throughput of MIMO-NCMA outperforms single-antenna NCMA and conventional distributed MIMO-MUD, respectively. We believe that MIMO-NCMA throughput can be further improved with modulations beyond QPSK (e.g., 64-QAM).**

I. Introduction

This paper studies a network-coded multiple access (NCMA) system with higher-order modulations beyond BPSK. NCMA, first proposed in [1], is a new multiple access wireless local area network (WLAN) system with multipacket reception capability. Fig. 1 shows a typical WLAN setup in which two end nodes send messages to the same access point (AP). To boost throughput, the two end nodes are allowed to send their packets simultaneously.

The key idea of NCMA is to combine physical-layer network coding (PNC) and multiuser decoding (MUD) to enable multipacket reception. PNC was first introduced in [2]. PNC turns mutual interference between simultaneous signals from different transmitters to useful network-coded information, thereby improving the throughput of wireless *relay* networks. Subsequent to [2], the authors of [1] explored the use of PNC decoding for *non-relay* networks (e.g., uplink of WLAN). MUD, on the other hand, has been widely studied in the past few decades [3].

In NCMA, each client (sender) node partitions and encodes one large source message to multiple small packets at the MAC layer [1]. At the PHY layer, additional channel coding is performed on each small packet before it is transmitted to the AP (see Fig. 2). At the AP, two PHY-layer decoders are used to decode useful information from overlapped packets transmitted simultaneously by different client nodes: (i) the PNC decoder attempts to decode a network-coded packet (e.g., binary XORed [2]), while (ii) the MUD decoder attempts to decode the individual original packets embedded within the overlapped signals. The decoded packets from multiple time slots, including the network-coded and individual packets, are then forwarded to the AP's MAC layer for the recovery of MAC-layer messages from the client nodes.



Fig. 1. System Model for NCMA.

Prior work on NCMA [1], [4] realized a simple NCMA prototype with BPSK modulation only. The normalized throughput of the BPSK NCMA system is bounded by 2 (i.e., 2 binary packets per unit time). To further increase the system throughput, especially in the medium and high signal-to-noise ratio (SNR) regimes, it is desirable to adopt higher-order modulations. However, as will be shown, direct generalization of the scheme in [1], [4] from BPSK to QPSK leads to very low system throughput. For example, rather than a boost, the system throughput actually drops from 1.2 to 0.2 at 9dB SNR (see Fig. 11 and elaboration in Section V) when we move from BPSK to QPSK.

This drastic throughput degradation is caused by the relative phase offset between the channel gains of simultaneously transmitted packets. Although certain advanced channel decoding methods expounded in the literature [5]–[7] may partially solve the phase offset problem for the PNC and MUD decoders, these are generally complex decoding methods that induce excessive latency; that is, they are not amenable to real-time operation. This paper, on the other hand, aims for high-order NCMA prototypes that operate in real time. We therefore opt to adapt the simpler conventional Viterbi decoders for the purpose of PNC and MUD decodings here, assuming the use of convolutional codes.

Direct extension of our previous BPSK PNC and MUD

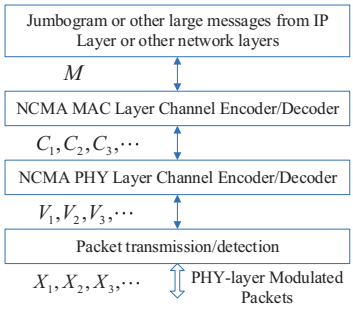


Fig. 2. The general architecture of a NCMA node's information processing at MAC and PHY layers.

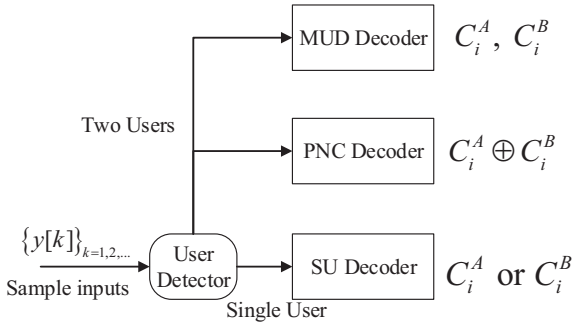


Fig. 3. NCMA PHY-layer channel decoders.

decoders in [1], [4] for QPSK does not work well. In this paper, we explore the use of two antennas at the AP to provide an additional degree of freedom to tackle the aforementioned relative phase offset problem. The client nodes still have only one antenna each. Although our setup may look like a distributed MIMO system, we remark that a typical distributed MIMO system only incorporates MUD decoding but not PNC decoding. We refer to our system as *MIMO-NCMA*.

To test the performance of MIMO-NCMA, we implemented it on software-defined radios. Our experimental results show that, at SNR of 10dB, the throughput of MIMO-NCMA outperforms those of conventional systems operated with distributed ZF and MMSE MIMO decoders by 100% and 80%, respectively. At the same time, MIMO-NCMA improves the throughput of the previous single-antenna NCMA system [1], [4] by nearly 100% for all SNRs.

Related Work

Physical-layer network coding: Ref. [2] first proposed PNC to increase the throughput of a two-way relay network (TWRN), where two end nodes exchange information via a relay. PNC doubles the throughput of a TWRN compared with the traditional scheme [2]. PNC has been studied and evaluated in depth: we refer the interested readers to [8]–[11] and the references thereof for details. Following the tradition of [2], prior PNC works focused almost exclusively on *relay* networks. By contrast, NCMA was the first attempt to apply PNC in *non-relay* networks [1], [4].

Coding for Multiple Access Channels: Besides NCMA [1], [4], there have been other efforts to apply network coding in multiple access networks. The major difference between NCMA and these works is that NCMA tries to decode more than one equation (e.g., both PNC packets and individual packets) from one overlapped packet, while most other works target to get one equation per reception (either PNC packets or one individual packet). Specifically, [12]–[14] explored forming linear equations from the collided packets to derive source packets by solving the linear equations. But [12], [14] only form one equation for each overlapped packet, whereas NCMA can have one or two equations for each overlapped packet depending on the channel condition. Also, the decoding in [13] is based on PHY-layer equations only. We are also aware of prior efforts in decoding source packets from collisions, e.g., Strider [15], AutoMAC [16]. However, [15] and [16] did not consider PNC decoding at the PHY layer.

Distributed MIMO-MUD: MIMO-NCMA is similar to distributed MIMO systems in that the AP has multiple antennas. Distributed MIMO can enable spatially separated transmitters to form a virtual MIMO system for multiple access. In the literature, [17]–[19] studied distributed MIMO systems to increase the system throughput, and we refer to them as MIMO-MUD since they focus on MUD decoder only. In this paper, we consider classical MIMO-MUD with zero-forcing (ZF), minimum mean square error (MMSE) decoders [20] as our benchmarks.

The remainder of the paper is organized as follows: Section II overviews the NCMA system. Section III studies the penalty induced by relative phase offsets in high-order modulation NCMA. Following that, Section IV puts forth our solutions. Section V presents the implementation details of our approach and the associated experimental results. Finally, Section VI discusses potential future works and Section VII concludes this paper.

II. Overview

A. General System Model for NCMA

We study a multiple access system where two end nodes, A and B, transmit information to an access point (AP) simultaneously, as shown in Fig. 1. We consider the use of both physical-layer network coding (PNC) and multiuser decoding (MUD) to boost system throughput. This system is referred to a network-coded multiple access (NCMA) system [1].

NCMA includes both MAC layer and PHY layer operations. With respect to Fig. 2, at the MAC layer, a large message M^A of node A is divided and encoded into multiple packets, $C_i^A, i = 1, 2, ...$ Similarly, a large M^B of node B is encoded into multiple packets, $C_i^B, i = 1, 2, ...$ We assume the use of Reed-Solomon (RS) code at the MAC layer when coding a large message into multiple packets. At the PHY layer, each packet C_i^A (or C_i^B) is further channel-encoded into V_i^A (V_i^B) for reliable transmission. We adopt the convolutional code as the PHY-layer channel codes.

Time Slot	A	$A \oplus B$	B
1	C_1^A	$C_1^{A\oplus B}$	C_1^B
2	C_2^A	ø	C_2^B
3	C_3^A	$C_3^{A\oplus B}$	ø
4	ø	$C_4^{A\oplus B}$	C_4^B
5	C_5^A	ø	ø
6	ø	ø	C_6^B
7	ø	$C_7^{A\oplus B}$	ø
8	ø	ø	ø

Fig. 4. An example of PHY-layer packet reception patterns for concurrently transmitted packets using PNC and MUD decoders. $\emptyset$ means the corresponding packets cannot be decoded.

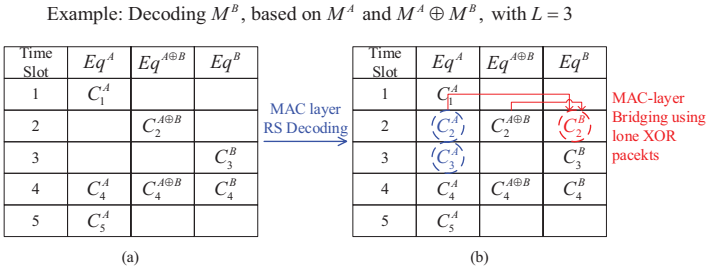


Fig. 5. NCMA MAC-layer decoding and bridging example, using L=3 RS code: (a) The decoding outcomes after PHY-layer bridging; (b) MAC-layer RS decoding and bridging using lone XOR packets.

NCMA is a time-slotted system. That is, each end node transmits packets $V_1, V_2, ..., V_i, ...$ to the AP in successive time slots, and the two end nodes' packets (i.e., V_i^A and V_i^B) are configured to transmit simultaneously in the same time slot i.

In the uplink transmission of NCMA, at the PHY layer, as shown in Fig. 3, the AP first detects how many nodes are transmitting. If only one node transmitting, the Single-User (SU) decoder will be selected. When two nodes transmit simultaneously, the AP receives a superimposed packet. In this case, the AP decodes using two multiuser decoders: the MUD decoder and the PNC decoder. The MUD decoder attempts to decode both packets C_i^A and C_i^B explicitly, and the PNC decoder attempts to decode a linear combination[1] of two packets C_i^A and C_i^B, i.e., $C_i^A \oplus C_i^B$. The packets from the PHY-layer decoders are collected from different time slots, and then passed to the MAC layer for further processing. With the help of the MAC-layer RS code, the AP decodes the original messages M^A and M^B.

B. An Example

Different from traditional multipacket reception systems where only MUD was adopted [3], a main distinguishing feature of NCMA is that it combines PNC decoding with MUD to improve the system throughput. In particular, it is possible that sometimes only a network-coded packet can be decoded using PNC decoding while MUD fails to recover either the packet from A or the packet from B. In this subsection, we introduce the advantages and key idea of NCMA using a simple example.

PHY-layer Bridging – Let us focus on the PHY-layer decoding outcomes first. For the MUD decoder, for a time slot i, there are four possible outcomes: (i) both C_i^A and C_i^B are successfully decoded; (ii) only C_i^A is successfully decoded; (iii) only C_i^B is successfully decoded; (iv) neither C_i^A nor C_i^B can be decoded. For the PNC decoder, there are two possible outcomes: (a) $C_i^A \oplus C_i^B$ is successfully decoded; (b) $C_i^A \oplus C_i^B$ cannot be decoded. As a result, we have $4 \times 2 = 8$ possible outcomes. We refer to these combined outcomes from PNC and MUD decoders as "events". Fig. 4 shows an example of the eight events of the PNC and MUD decoders, assumed to occur in eight successive time slots. In time slots 3 and 4, where C_3^A and $C_3^A \oplus C_3^B$ (abbreviated as $C_3^{A\oplus B}$), C_4^B and $C_4^A \oplus C_4^B$ (abbreviated as $C_4^{A\oplus B}$) are decoded, complementary XOR packets $C_3^{A\oplus B}$ and $C_4^{A\oplus B}$ can be used to recover individual missing packets C_3^B and C_4^A, respectively. This process, which leverages the complementary XOR packets, is referred to as PHY-layer bridging [1].

MAC-layer Bridging – In Fig. 4, PHY-layer bridging cannot be applied to time slot 7 because neither native packet C_7^A nor C_7^B is available, and only a lone network-coded packet $C_7^{A\oplus B}$ (namely, PNC packet) is decoded. In NCMA, such lone PNC packets turn out to be useful in MAC-layer decoding. Fig. 5 gives an example illustrating the main idea. Fig. 5(a) shows the PHY-layer decoding outcomes for a number of successive time slots. We assume the AP has recovered enough number of native packets C_i^A to decode M^A with the help of the MAC-layer RS code by time slot 5 – in this example, $L = 3$ PHY-layer packets are needed to recover M^A. With MAC-layer decoding, native packets C_2^A and C_3^A can also be decoded (conceptually, we could obtain C_2^A and C_3^A based on re-encoding the recovered M^A at the MAC-layer, although in practice, a simpler process is possible). Note that the PHY layer failed to obtain C_2^A in time slot 2, but the MAC layer recovers it in time slot 5. With C_2^A, the original lone PNC packet $C_2^A \oplus C_2^B$ in time slot 2 becomes a complementary XOR packet. Consequently, we can recover C_2^B (using C_2^A and $C_2^A \oplus C_2^B$), and therefore node B now have enough native packets (i.e., $L = 3$) to recover message, as shown in Fig. 5(b). We refer this process as MAC-layer bridging, which further boosts the system throughput by leveraging the lone PNC packets [1].

III. Single Antenna System

Section II showed that NCMA can extract useful information from the concurrently transmitted packets through PHY-layer bridging and MAC-layer bridging. Previous works on NCMA [1], [4] adopted single antenna at the AP with BPSK modulation, and therefore the system throughput was upper-bounded by two bits per channel use, i.e., at most two bits could be decoded per channel use by the AP in the high signal-to-noise ratio (SNR) regime. To further

[1]In this paper, we only consider the bit-wise eXclusive-OR (XOR), $\oplus$, operation of C_i^A and C_i^B.

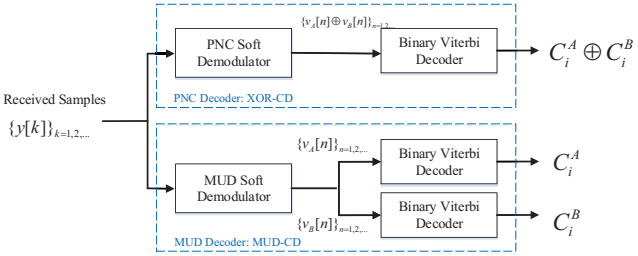


Fig. 6. NCMA PHY-layer PNC decoder (XOR-CD) and MUD decoder (MUD-CD) for simultaneous transmissions from two nodes.

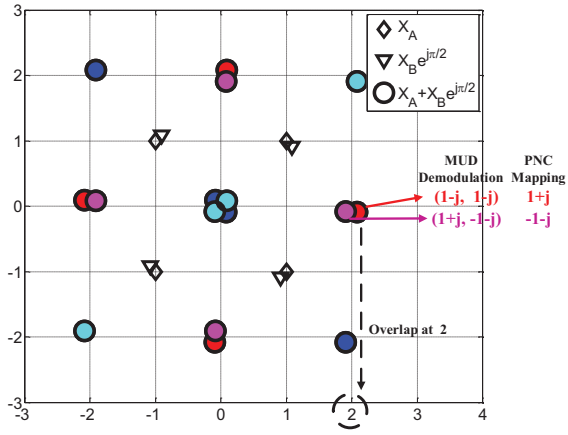


Fig. 7. Constellation map for the received samples at the AP for $|h_A| = |h_B| = 1$ and relative phase offset $\Delta\phi = \pi/2$. Note that, we purposely set $\Delta\phi$ to be slightly smaller than $\pi/2$ to highlight different PNC mappings using different colors, where the same color corresponds to the same network-coded symbol. The symbol pair (x_A, x_B) denotes the MUD demodulated symbols.

boost the NCMA system throughput, especially at medium-high SNRs (e.g., SNR $\geq$ 10dB), this paper considers higher-order modulations to avoid the saturation of data rate [21].

In [4], both PHY and MAC layer real-time decoders have been evaluated on the software-defined radio platform. To support real-time processing at the PHY layer, XOR-CD and MUD-CD [8] are chosen as the PNC and MUD decoders, respectively (details of XOR-CD and MUD-CD can be found in the following two subsections). A salient feature of these decoders is that the standard low-complexity point-to-point binary Viterbi channel decoder can be used with changes on the demodulators only, as shown in Fig. 6 (see [4] for details). However, as will be elaborated, both PNC and MUD decoders encounter a critical phase problem when we move from BPSK to higher-order modulations. In the following, we illustrate with XOR-CD and MUD-CD on QPSK as examples.

A. Phase Penalty for PNC Decoder

Several decoding approaches are possible for channel-coded PNC systems [8]. In this paper, since we aim for real-time operations rather than optimal performance, we use the simple XOR-CD decoder as the PNC decoder. Sophisticated PNC decoders with better BER performance are possible, at the cost of high computational complexity and large decoding delays, e.g., Jt-CNC (joint channel and network decoding) [6]. They have been studied in the literature, and we refer interested readers to [5], [8] for further details.

The general architecture for XOR-CD is shown in the upper block of Fig. 6. Let $V^A = (v_A[1], ..., v_A[n], ...)$ denote the PHY-layer codeword of node A in one time slot (i.e., one binary encoded packet), where $v_A[n] \in \{0, 1\}$ is the n-th convolutional encoded bit (similarly, we have $V^B = (v_B[1], ..., v_B[n], ...)$ for node B). Assuming QPSK modulation, the k-th modulated symbol $x_A[k]$ for the PHY-layer transmitted packet $X^A = (x_A[1], ..., x_A[k], ...)$ can be expressed as

$$x_A[k] = (1 - 2v_A[2k-1]) + (1 - 2v_A[2k])j, \;\; k = 1, 2, 3, ... \tag{1}$$

Let us assume an OFDM system where multipath fading can be dealt with by cyclic prefix (CP). The k-th received sample in the frequency domain at the AP can be written as

$$y_R[k] = h_A[k]x_A[k] + h_B[k]x_B[k] + w[k], \tag{2}$$

where $w[k]$ is the noise term, and $h_A[k]$, $h_B[k]$ are the channel gains of the k-th samples of nodes A and B, respectively. In XOR-CD, the received samples $\{y_R[k]\}_{k=1,2,3,...}$ are first passed through the PNC demodulator to obtain the XOR bits $\{v_A[n] \oplus v_B[n]\}_{n=1,2,...}$. Note that the outputs $\{v_A[n] \oplus v_B[n]\}_{n=1,2,...}$ from the PNC demodulator can be hard or soft bits. These bits are then fed to a standard binary Viterbi decoder (as used in a point-to-point system) to decode the network-coded packet $C_i^A \oplus C_i^B$. The standard Viterbi decoder can be used for PNC decoding because XOR-CD exploits the linearity of linear channel codes, such as convolutional codes. Specifically, define $\Pi(\cdot)$ as the convolutional channel encoder. Since $\Pi(\cdot)$ is linear, we have $V^A \oplus V^B = \Pi\left(C^A\right) \oplus \Pi\left(C^B\right) = \Pi\left(C^A \oplus C^B\right)$.

With respect to node A, the odd (even) bits of V^A are mapped to the real (imaginary) part of $x_A[k]$ in QPSK, i.e., $x_A^I[k] = 1 - 2v_A[2k-1]$ ($x_A^Q[k] = 1 - 2v_A[2k]$). A particular pair of symbols from the two nodes is expressed as $(x_A[k],\ x_B[k]) = (x_A^I[k] + x_A^Q[k]j,\ x_B^I[k] + x_B^Q[k]j)$.

An important issue in PNC is how to calculate $x_A[k] \oplus x_B[k]$ (abbreviated as $x_{A\oplus B}[k]$) using the received sample $y_R[k]$ in (2). To maintain the linear property of convolutional codes, in XOR-CD we need to map the real part of $x_A[k]$ with the real part of $x_B[k]$, i.e., $x_A^I[k]$ with $x_B^I[k]$ (similarly, $x_A^Q[k]$ with $x_B^Q[k]$) into a network-coded real (imaginary) part of $x_{A\oplus B}[k]$. More precisely, the PNC mapping in XOR-CD for $x_{A\oplus B}[k]$ is defined as

$$x_{A\oplus B}[k] = x_A^I[k] \oplus x_B^I[k] + x_A^Q[k] \oplus x_B^Q[k]j, \tag{3}$$

where $x_A^I[k] \oplus x_B^I[k] = x_A^I[k]x_B^I[k]$ and $x_A^Q[k] \oplus x_B^Q[k] = x_A^Q[k]x_B^Q[k]$ given that $x_A^I[k], x_B^I[k], x_A^Q[k], x_B^Q[k] \in \{1, -1\}$. The PNC demodulation rule for the XORed bits

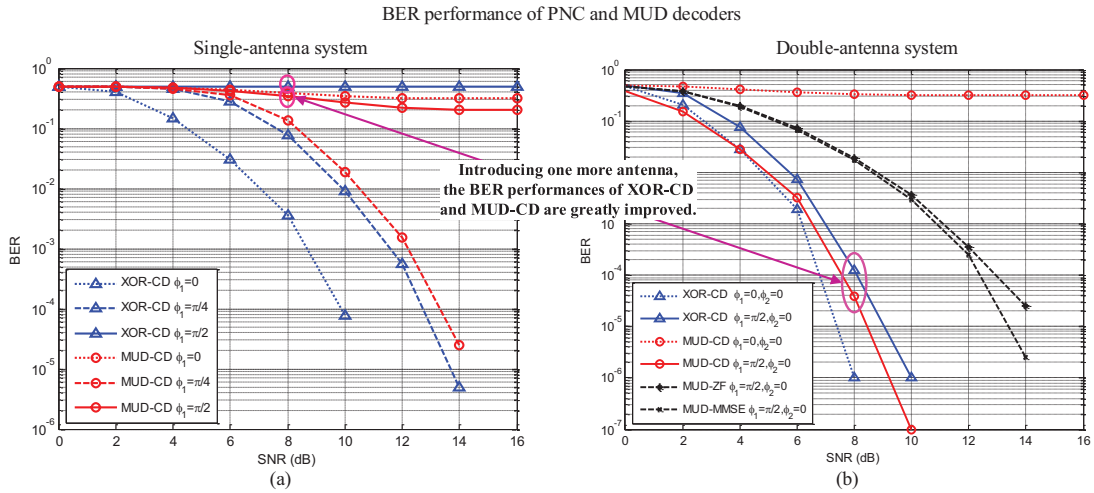


Fig. 8. BER results for single-antenna and double-antenna NCMA systems with different relative phase offsets in AWGN channels: (a) single antenna XOR-CD and MUD-CD decoders; (b) XOR-CD and MUD-CD decoders two antennas, benchmarked by ZF (zero-forcing) and MMSE (minimum mean square error) decoders.

is defined as

$$v_A[2k-1] \oplus v_B[2k-1] = \frac{1 - x_A^I[k] \oplus x_B^I[k]}{2},$$
$$v_A[2k] \oplus v_B[2k] = \frac{1 - x_A^Q[k] \oplus x_B^Q[k]}{2}. \quad (4)$$

Let us focus on one particular received sample $y_R[k] = x_A[k] + x_B[k]e^{j\Delta\phi}$, where $\Delta\phi$ is the relative phase offset between the two nodes (assuming perfect power control so that the received signal powers for both nodes are equal, and we have $h_A[k] = 1$ and $h_B[k] = e^{j\Delta\phi}$). Fig. 7 plots the noise-free constellation map for $\Delta\phi = \pi/2$, in which some constellation points overlap with the others (note: to see the overlapping constellations points more clearly in the figure, we purposely set $\Delta\phi$ to be slightly smaller than $\pi/2$). In Fig. 7, constellation points of the same color are mapped to the same XOR value. Note for example that the constellation points of symbol pairs $(1-j, 1-j)$ and $(1+j, -1-j)$ overlap, but they are mapped to different XOR values. In particular, when $\Delta\phi = \pi/2$, the XOR mapping of (3) leads to ambiguity even in the absence of noise, and the error probability for the network-coded symbol can be as high as 50%.

From the simulation results in Fig. 8(a), we can see that the BER performance of XOR-CD with $\Delta\phi = \pi/2$ degrades greatly compared with that of $\Delta\phi = \pi/4$. In general, we find that the BER performance of XOR-CD is determined by the relative phase offset $\Delta\phi$. Interestingly, as will be detailed in the next subsection, the BER performance of MUD-CD is also highly correlated with the relative phase offset $\Delta\phi$.

B. Phase Penalty for MUD Decoder

The architecture of MUD-CD is shown in the lower block of Fig. 6. The goal of the MUD-CD decoder is to decode two source packets C_i^A and C_i^B separately. In this process, the received samples $\{y_R[k]\}_{k=1,2,3,...}$ are first passed through a MUD demodulator to get the binary channel-encoded bits $\{v_A[n]\}_{n=1,2,...}$ and $\{v_B[n]\}_{n=1,2,...}$, which are then fed into two binary Viterbi decoders to recover the packets C_i^A and C_i^B of nodes A and B, respectively.

Let us use the constellation map in Fig. 7 to explain the phase penalty problem for MUD-CD. With respect to a particular constellation point "2", we cannot distinguish between the symbol pair $(1-j, 1-j)$ and symbol pair $1+j, -1-j)$, based on the received sample $y_R[k]$ when $\Delta\phi = \pi/2$. From the BER curves in Fig. 8(a), we can see that the BER performance of XOR-CD is also related to the relative phase offset $\Delta\phi$ between two nodes. We find that both PNC and MUD decoders' BER performances degrade drastically when $\Delta\phi = \pi/2$. In general, when $\Delta\phi$ is in the range of $\pi/4 \le \Delta\phi \le 3\pi/4$ or $5\pi/4 \le \Delta\phi \le 7\pi/4$, the PNC mapping (3) degrades the performance of XOR-CD decoder; when $\Delta\phi = m\pi/2, m = 0, 1, 2, ...$, the overlapping constellation points degrade the performance of MUD-CD decoder. This is a hurdle for NCMA systems when QPSK is adopted. This hurdle can be overcome with the use of multiple antennas at the AP, as explained in Section III-C.

C. Possible Solutions to Alleviate Phase Penalty

The fundamental reason why the BER performance of NCMA is bad when $\Delta\phi = \pi/2$ is that some overlapping constellation points are to be mapped into different network-coded symbols for PNC decoding, or to be demodulated into two different symbol pairs for MUD decoding. In the literature, there are several approaches that could partially solve the phase penalty problem for PNC system. For example, [8] proposed a real-to-imaginary PNC mapping for $x_{A\oplus B}$ (i.e., $x_A^I \oplus x_B^Q + x_A^Q \oplus x_B^I j$ rather than using (3) when the phase offset is $\pi/4 \le \Delta\phi \le 3\pi/4$ and the data are not channel-coded. However, the linearity

of convolutional codes will be destroyed by such irregular PNC mapping in a channel-coded PNC system, invalidating this method. Another possible method was put forth by [7], in which a QPSK to 5-QAM demodulation was adopted. This method, however, is not suitable for our XOR-CD system where only QPSK modulation is considered. [5], [6] studied a high computational-complexity Jt-CNC (joint channel-decoding and physical-layer network coding) approach that is not suitable for our real-time NCMA system as well.

Nowadays, APs are usually equipped with two or more antennas [22], [23]. This inspires us to tackle the phase penalty problem by making full use of multiple antennas. In the following, we consider an NCMA system in which the AP has multiple antennas, referred as MIMO-NCMA.

Assuming the relative phase offsets between the two transmitted packets of the two antennas at the AP are $\Delta\phi_1$ and $\Delta\phi_2$, respectively, Fig. 8(b) plots the BER curves of PNC and MUD decoders for $\Delta\phi_1 = 0$ and $\pi/2$, $\Delta\phi_2 = 0$ (details of MIMO-NCMA can be found in Section IV). When $\Delta\phi_1 = \Delta\phi_2 = 0$, MUD-CD reaches a 30% BER floor for individual packets, while XOR-CD works very well for the XOR packets. When the phase offset in the first antenna changes from 0 to $\pi/2$, we can see that the BER performances of both XOR-CD and MUD-CD decoders are greatly improved compared with the single antenna case with a $\Delta\phi_1 = \pi/2$ phase offset.

For benchmarking purposes, we also consider two classical distributed MIMO MUD decoders, namely the zero-forcing (ZF) decoder and the minimum mean square error (MMSE) decoder [20]. In the following, we will present our proposed higher-order modulated NCMA PHY-layer XOR-CD and MUD-CD decoders.

IV. Higher-order Modulation PHY-layer Decoders in MIMO-NCMA

This section presents the PHY-layer decoders for MIMO-NCMA: Section IV-A focuses on the design of the XOR-CD decoder, and Section IV-B, the MUD-CD decoder.

For the PHY-layer channel codes, our system adopts the same $[133, 171]_8$ convolutional code as in the 802.11 standard [22]. We aim for a simple decoder design to support real-time processing, and therefore, the simple XOR-CD and MUD-CD decoders presented in the Section III are chosen. Specifically, the single-antenna XOR-CD and MUD-CD decoders in Section III are adapted to be the corresponding MIMO XOR-CD and MUD-CD decoders.

A. PNC Decoder (XOR-CD)

Assume that the received samples on the two antennas at the relay are $\{y_{R1}[k]\}_{k=1,2,3,...}$ and $\{y_{R2}[k]\}_{k=1,2,3,...}$, respectively. Our target is to compute the log-likelihood ratios (LLR) of two bits $v_A[2k-1] \oplus v_B[2k-1]$ and $v_A[2k] \oplus v_B[2k]$ based on the k-th received samples $y_{R1}[k]$ and $y_{R2}[k]$ of antennas 1 and 2, assuming there is no bit-level interleaver on the outputs bits of the convolutional encoder. The PNC demodulator's outputs (namely, the soft

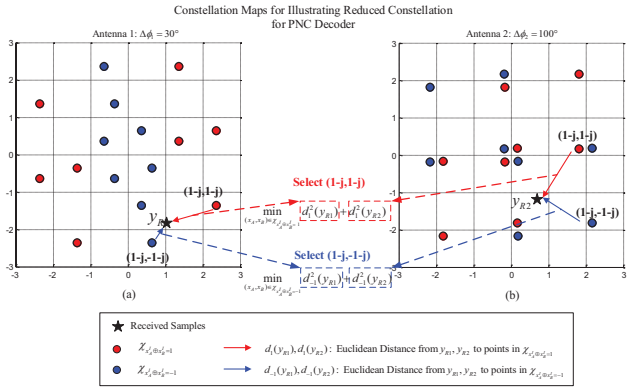


Fig. 9. Illustration of reduced-constellation scheme for PNC to obtain the soft information on $x_A^I \oplus x_B^I$: (a) Constellation map for antenna 1 with relative phase offset $\Delta\phi_1 = 30°$, (b) Constellation map for antenna 2 with relatvie phase offset $\Delta\phi_1 = 100°$. The black stars represent the received samples; red dots represent constellation points in $\chi_{x^I_{A\oplus B}=1}$ and blue dots for $\chi_{x^I_{A\oplus B}=-1}$. Red and blue solid lines represent the Euclidean distances from received samples to the constellation points originated from the sets $\chi_{x^I_{A\oplus B}=1}$ and $\chi_{x^I_{A\oplus B}=-1}$. We select the two constellation points by jointly considering two maps, i.e., the minimum sum of two Euclidean distances' square (dashed lines). In this example, $(1-j, 1-j)$ is selected in $\chi_{x^I_{A\oplus B}=1}$, and $(1-j, -1-j)$ is selected in $\chi_{x^I_{A\oplus B}=-1}$. These two selected constellation points correspond to two different values of $x_A^I \oplus x_B^I$.

information of $\{v_A[n] \oplus v_B[n]\}_{n=1,2,...}$) are fed into the Viterbi decoder. This subsection derives the soft information of $\{v_A[n] \oplus v_B[n]\}_{n=1,2,...}$.

We assume the end nodes use QPSK modulation and express the transmitted symbols as $x_A = x_A^I + x_A^Q j$ and $x_B = x_B^I + x_B^Q j$. The received frequency-domain samples (our NCMA system is an OFDM system) on the two antennas of the AP are

$$\begin{aligned} y_{R1} &= h_{A1}x_A + h_{B1}x_B + w_1 \\ y_{R2} &= h_{A2}x_A + h_{B2}x_B + w_2 \end{aligned} \tag{5}$$

where h_{A1} and h_{B1} (h_{A2} and h_{B2}) are the uplink channel gains of nodes A and B associated with the first (second) antenna, respectively, and w_1, w_2 are additive white Gaussian noises (AWGN) with variances σ_1^2 and σ_2^2.

Define the real component's LLR of packet A (i.e., x_A)'s QPSK symbol as $\log(P_A^I/Q_A^I)$, where P_A^I and Q_A^I are the probabilities for the real component of x_A to be 1 and -1, respectively. Similarly, for $LLR(x_A^I \oplus x_B^I)$, $P_{A\oplus B}^I$ and $Q_{A\oplus B}^I$ are the probabilities corresponding to $x_A^I \oplus x_B^I = 1$ and $x_A^I \oplus x_B^I = -1$. We have

$$\begin{aligned} LLR(x_A^I \oplus x_B^I) = \log \frac{P_{A\oplus B}^I}{Q_{A\oplus B}^I} &= \log P_{A\oplus B}^I - \log Q_{A\oplus B}^I \\ &= \log \Pr(x_A^I \oplus x_B^I = 1 | y_{R1}, y_{R2}) \\ &\quad - \log \Pr(x_A^I \oplus x_B^I = -1 | y_{R1}, y_{R2}). \end{aligned} \tag{6}$$

Out of the 16 constellation points associated with the symbol pair (x_A, x_B), eight correspond to $x_A^I \oplus x_B^I = 1$ (the red dots in Fig. 9), and eight correspond to $x_A^I \oplus x_B^I = -1$

(the blue dots in Fig. 9). Let $\chi_{x^I_{A\oplus B}=1}$ denote the set of symbol pairs (x_A, x_B) that satisfy $x^I_A \oplus x^I_B = 1$[2]. We can express $P^I_{A\oplus B}$ as

$$P^I_{A\oplus B} = \Pr(x^I_A \oplus x^I_B = 1 | y_{R1}, y_{R2}) \propto \sum_{(x_A,x_B)\in\chi_{x^I_A\oplus x^I_B=1}} \exp\{-\frac{|y_{R1}-h_{A1}x_A-h_{B1}x_B|^2}{\sigma_1^2}\} \cdot \exp\{-\frac{|y_{R2}-h_{A2}x_A-h_{B2}x_B|^2}{\sigma_2^2}\}. \quad (7)$$

We compute $Q^I_{A\oplus B}$ in a similar way based on the set $\chi_{x^I_{A\oplus B}=-1}$. After that, we substitute $P^I_{A\oplus B}$ and $Q^I_{A\oplus B}$ into the LLR expression of (6) to get (8).

Fig. 9 plots the constellation maps of the two antennas with the same uplink channel-gain magnitude but with relative phase offsets $\Delta\phi_1 = 30°$ and $\Delta\phi_1 = 100°$ on antennas 1 and 2. Constellation points of sets $\chi_{x^I_{A\oplus B}=1}$ and $\chi_{x^I_{A\oplus B}=-1}$ are marked by red and blue dots, respectively. In MIMO-NCMA, for further simplification, when computing $LLR(x^I_A \oplus x^I_B)$, we first reduce the number of constellation points from 16 to 2, i.e., choose only one constellation point in $\chi_{x^I_{A\oplus B}=1}$ and one in $\chi_{x^I_{A\oplus B}=-1}$ (see the red and blue arrows of Fig. 9). The two selected constellation points correspond to the most likely points representing two different XOR values of $x^I_A \oplus x^I_B$. After that, we compute the LLR based on the two selected constellation points (see the dashed blocks between the two figures). We refer to this demodulation procedure as reduced constellation demodulation scheme.

We remark that each antenna gives us a soft information of $x^I_A \oplus x^I_B$. How to combine the two soft information from two antennas into one complete soft input for the Viterbi decoder is our key concern, which will be elaborated in the following.

Reduced-constellation Demodulation for Two Antennas

We assume the noise variances σ_1^2 and σ_2^2 to be the same, $\sigma_1^2 = \sigma_2^2 = \sigma^2$. Note that, in real wireless systems, σ_1^2 and σ_2^2 may not be equal sometimes; however, our derivations below can be easily generalized to deal with the case $\sigma_1^2 \neq \sigma_2^2$. We adopt the log-max approximation, $\log(\sum_i exp(z_i)) \approx \max_i z_i$ [10], to simplify the LLR calculation. For example, $\log P^I_{A\oplus B}$ can be expressed as (9), where $d_1(y_{R1}) = |y_{R1} - h_{A1}x_A - h_{B1}x_B|$ and $d_1(y_{R2}) = |y_{R2} - h_{A2}x_A - h_{B2}x_B|$ are the Euclidean distances from y_{R1} and y_{R2} to the constellation point (x_A, x_B) in $\chi_{x^I_{A\oplus B}=1}$. The physical meaning of (9) can be understood to be selecting one point with the minimum $d_1^2(y_{R1}) + d_1^2(y_{R2})$ value among all symbol pairs in set $\chi_{x^I_{A\oplus B}=1}$.

Similarly, define $d_{-1}(y_{R1})$ and $d_{-1}(y_{R2})$ as the Euclidean distance from y_{R1} and y_{R2} to points in $\chi_{x^I_{A\oplus B}=-1}$, respectively. In Fig. 9, $(1-j, 1-j)$ is selected in $\chi_{x^I_{A\oplus B}=1}$,

[2]The set $\chi_{x^I_{A\oplus B}=1}$ contains eight constellation points originated from the symbol pair (x_A, x_B), namely, $(1+j, 1+j), (1+j, 1-j), (-1+j, -1+j), (-1+j, -1-j), (1-j, 1+j), (1-j, 1-j), (-1-j, -1+j)$ and $(-1-j, -1-j)$.

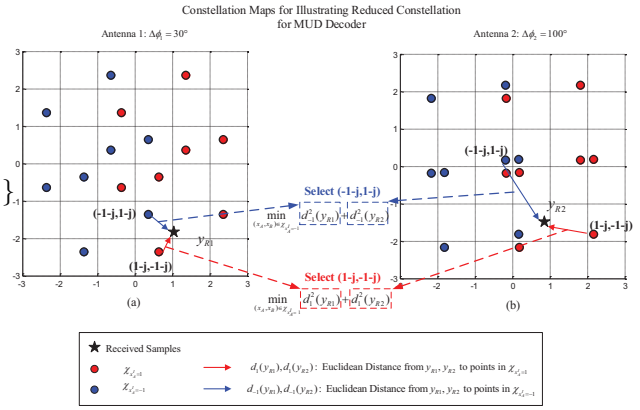


Fig. 10. Illustration of the reduced-constellation scheme for MUD to obtain soft information on x^I_A: Red and blue solid lines represent the Euclidean distances from received samples to the constellation points originated from the sets $\chi_{x^I_A=1}$ and $\chi_{x^I_A=-1}$. In this example, $(1-j, -1-j)$ is selected in $\chi_{x^I_A=1}$, and $(-1-j, 1-j)$ is selected in $\chi_{x^I_A=-1}$. These two selected constellation points correspond to two different values of x^I_A.

and $(1-j, -1-j)$ is selected in $\chi_{x^I_{A\oplus B}=-1}$ to represent the cases of $x^I_A \oplus x^I_B = 1$ and $x^I_A \oplus x^I_B = -1$, respectively. The approximation of $LLR(x^I_A \oplus x^I_B)$ is

$$LLR(x^I_A \oplus x^I_B) \approx \min_{(x_A,x_B)\in\chi_{x^I_{A\oplus B}=1}} \{d_1^2(y_{R1}) + d_1^2(y_{R2})\} - \min_{(x_A,x_B)\in\chi_{x^I_{A\oplus B}=-1}} \{d_{-1}^2(y_{R1}) + d_{-1}^2(y_{R2})\}. \quad (10)$$

The QPSK demodulation from $x^I_A[k] \oplus x^I_B[k]$ to $v_A[2k-1] \oplus v_B[2k-1]$ is a one-to-one mapping (see (4)), and it is easy to show that the following LLR relationship always holds:

$$LLR(v_A[2k-1] \oplus v_B[2k-1]) = \log \frac{P^I_{A\oplus B}}{Q^I_{A\oplus B}} = LLR(x^I_A[k] \oplus x^I_B[k]). \quad (11)$$

Similarly, $LLR(x^Q_A[k] \oplus x^Q_B[k])$ can expressed by the even input bits' $LLR(v_A[2k] \oplus v_B[2k])$.

B. MUD Decoder (MUD-CD)

The MUD decoder for MIMO-NCMA follows the same reduced constellation principle as that of the PNC decoder, with the difference that its target is to obtain the individual soft information of $\{v_A[n]\}_{n=1,2,...}$ and $\{v_B[n]\}_{n=1,2,...}$ rather than their XOR.

Without loss of generality, let us focus on the derivation of the soft information for packet A. $LLR(x^I_A[k])$ and $LLR(x^Q_A[k])$ are the soft information for $v_A[2k-1]$ and $v_A[2k]$, respectively. Based on the sets of $\chi_{x^I_A=1}$[3] and $\chi_{x^I_A=-1}$, $LLR(x^I_A)$ can be expressed as (12).

[3]The set $\chi_{x^I_A=1}$ also contains eight constellation points originated from the symbol pair (x_A, x_B), namely, $(1+j, 1+j), (1+j, 1-j), (1+j, -1+j), (1+j, -1-j), (1-j, 1+j), (1-j, 1-j), (1-j, -1+j)$ and $(1-j, -1-j)$

$$LLR(x_A^I \oplus x_B^I) \propto \log \sum_{(x_A,x_B)\in\chi_{x_A^I \oplus x_B^I=1}} \exp\{-\frac{|y_{R1}-h_{A1}x_A-h_{B1}x_B|^2}{\sigma_1^2}\}\cdot\exp\{-\frac{|y_{R2}-h_{A2}x_A-h_{B2}x_B|^2}{\sigma_2^2}\}$$
$$-\log \sum_{(x_A,x_B)\in\chi_{x_A^I \oplus x_B^I=-1}} \exp\{-\frac{|y_{R1}-h_{A1}x_A-h_{B1}x_B|^2}{\sigma_1^2}\}\cdot\exp\{-\frac{|y_{R2}-h_{A2}x_A-h_{B2}x_B|^2}{\sigma_2^2}\}. \quad (8)$$

$$\begin{aligned}\log P_{A\oplus B}^I &\propto \max_{(x_A,x_B)\in\chi_{x_{A\oplus B}^I=1}} \{-|y_{R1}-h_{A1}x_A-h_{B1}x_B|^2-|y_{R2}-h_{A2}x_A-h_{B2}x_B|^2\}\\ &\propto \min_{(x_A,x_B)\in\chi_{x_{A\oplus B}^I=1}} \{|y_{R1}-h_{A1}x_A-h_{B1}x_B|^2+|y_{R2}-h_{A2}x_A-h_{B2}x_B|^2\}\\ &\propto \min_{(x_A,x_B)\in\chi_{x_{A\oplus B}^I=1}} \{d_1^2(y_{R1})+d_1^2(y_{R2})\}. \end{aligned} \quad (9)$$

$$LLR(x_A^I) \propto \log \sum_{(x_A,x_B)\in\chi_{x_A^I=1}} \exp\{-\frac{|y_{R1}-h_{A1}x_A-h_{B1}x_B|^2}{\sigma_1^2}\}\cdot\exp\{-\frac{|y_{R2}-h_{A2}x_A-h_{B2}x_B|^2}{\sigma_2^2}\}$$
$$-\log \sum_{(x_A,x_B)\in\chi_{x_A^I=-1}} \exp\{-\frac{|y_{R1}-h_{A1}x_A-h_{B1}x_B|^2}{\sigma_1^2}\}\cdot\exp\{-\frac{|y_{R2}-h_{A2}x_A-h_{B2}x_B|^2}{\sigma_2^2}\}. \quad (12)$$

Following the same "log-max approximation" rule as in (9), we now have the approximation of $LLR(x_A^I)$:

$$\begin{aligned}LLR(x_A^I) \approx &\min_{(x_A,x_B)\in\chi_{x_A=1}} \{d_1^2(y_{R1})+d_1^2(y_{R2})\}\\ &-\min_{(x_A,x_B)\in\chi_{x_A^I=-1}} \{d_{-1}^2(y_{R1})+d_{-1}^2(y_{R2})\}.\end{aligned} \quad (13)$$

Fig. 10 shows a reduced constellation example for MUD-CD using the same constellation map of Fig. 9. We note that for the same constellation map and the same received samples, the soft outputs of XOR-CD decoder and MUD-CD decoder are in general different. For example, the XOR-CD decoder selects two points $(1-j, 1-j)$ and $(1-j, -1-j)$ to compute $LLR(x_A^I \oplus x_B^I)$, which implies that we have already made a decision that $x_A^I = 1$ (i.e., the $LLR(x_A^I)$ is infinite). However, the MUD-CD decoder selects $(1-j, -1-j)$ and $(-1-j, 1-j)$ to compute $LLR(x_A^I)$. In this example, the PNC decoder's LLR for x_A^I is higher than that of the MUD decoder. In a real wireless system, since the constellation map changes from one sample to another sample, sometimes the MUD decoder's LLR may be higher, and sometimes the PNC's LLR. NCMA can best utilize and extract useful information out of the received samples, by jointly making use of PNC and MUD decoders.

V. Experimental Results

To evaluate the performance of our proposed higher-order NCMA system, we implemented it on software-defined radios. Section V-A presents the implementation details and experimental setup and Section V-B presents the experimental results.

A. Implementation Details and Experimental Setup

The MIMO-NCMA system was built on the USRP hardware [24] and the GNU Radio software with the UHD driver. We extended the single-antenna BPSK NCMA system in [4] as follows:

a) We added one more antenna at the AP and changed the SISO system of [4] so that the AP can receive data from the two antennas in a MIMO way. The end nodes still use one antenna.
b) We modified the transceiver design so as to support QPSK modulation in addition to BPSK modulation.
c) We realized the QPSK XOR-CD and MUD-CD decoders based on the reduced-constellation demodulation scheme.

For experimentation, we deployed three sets of USRP N210s with SBX daughterboard boards. Each MIMO-NCMA node is a USRP connected to a PC through an Ethernet cable. For the uplink channel, the AP polls two nodes to transmit together (i.e., the AP sends beacon frames to trigger nodes A and B's packets). Our experiments were carried out at 2.585GHz with 5MHz bandwidth.

The following three systems are considered for benchmarking purpose:

1) *Single-antenna NCMA system (Single-NCMA)*
This system is based on the previous single-antenna NCMA system [4] and it serves as a benchmark here. We extend the system in [4] to support QPSK modulation in addition to BPSK modulation. Both MUD decoder and PNC decoder are used. PHY-layer bridging and MAC-layer bridging are performed in the decoding process to increase the system through-

put. In this system, all nodes have only one antenna each.

2) *Distributed MIMO System (MIMO-MUD)*
This is a distributed QPSK MIMO-MUD system, where the receiver at the AP has two antennas and the transmitters at the two end nodes have only one antenna each. Conventional hard-input-hard-output ZF (zero-forcing) and MMSE (minimum mean square error) decoders are adopted [20] for MUD decoding.
3) *MIMO NCMA system (MIMO-NCMA)*
This is the QPSK NCMA system proposed in the paper. Both XOR-CD and MUD-CD decoders are adopted, allowing the use of PHY-layer and MAC-layer bridgings to boost the system throughput.

B. Experimental Results

We study both PHY-layer and MAC-layer performances of our MIMO-NCMA system: we first consider the PHY layer packet error rate (PER) of PNC and MUD decoders, and then evaluate the MAC layer throughput when both PHY-layer and MAC-layer bridgings are incorporated.

1) PHY-layer Decoding Statistics: We collected the PHY-layer statistics for the above three systems, namely NCMA, MIMO-MUD and MIMO-NCMA, and present the results in Fig. 11. There are eight possible decoding outcomes (events, see Section II-B) when PNC and MUD decoders are used jointly (in Single-NCMA and MIMO-NCMA systems). We group some events together as follows:

- `NONE` = (iv)(b) (no packet decoded).
- `X` = (iv)(a) (only XOR packet decoded).
- `A|B` = (ii)(b) + (iii)(b) (either only packet A or only packet B decoded).
- `AX|BX` = (ii)(a) + (iii)(a) (XOR packet plus either packet A or packet B decoded).
- `AB` = (i)(b) (both packets A and B decoded; XOR packet not decoded).
- `ABX` = (i)(a) (both packets A and B decoded; XOR packet decoded).

We performed controlled experiments for different received SNRs, and the received powers of signals from nodes A and B at the AP were adjusted to be approximately balanced (note here that the powers of each pair can be slightly different due to channel fading, and the SNR is the average SNR of all the received packets). We calculated the SNR using the scheme in [21], and varied the SNR values from 6.5 to 9dB when the AP has single antenna. When the AP has two antennas, we varied the SNR values from 9 to 11.5dB since the received power is almost double [20]. For each SNR, the AP sent 1,000 beacon frames to trigger simultaneous transmissions of two end nodes.

Observation 1: Single-NCMA fails to support QPSK

Sections III-A and III-B have discussed the potential phase penalty associated with PNC and MUD decoders when QPSK is adopted in a single-antenna NCMA system. Our experimental results corroborate the theoretical and simulation analysis. The PHY-layer decoding statistics in

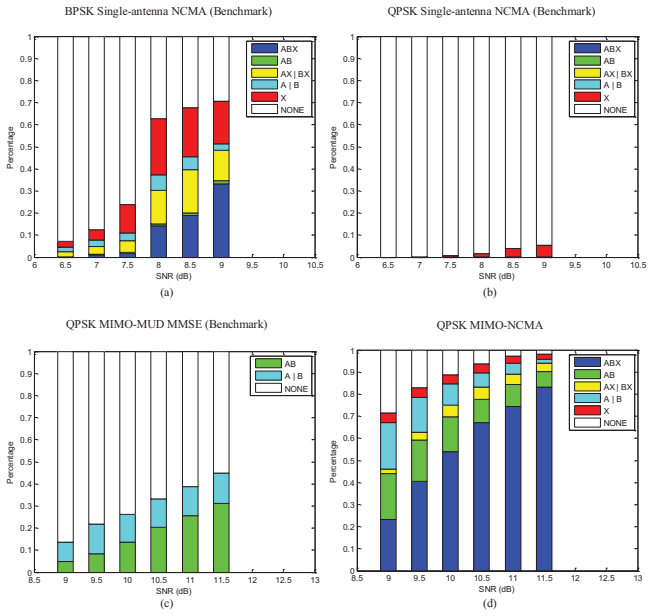


Fig. 11. PHY-layer packet statistics versus SNR for different decoding schemes with balanced received powers of two end nodes: (a) BPSK Single-NCMA; (b) QPSK Single-NCMA; (c) QPSK MIMO-MUD (MMSE); (d) QPSK MIMO-NCMA.

Fig. 11(b) shows that both PNC and MUD decoders cannot work well. Even at 9dB SNR (the working region for a point-to-point QPSK WLAN system [21]), there are almost no decoded packets.

Observation 2: MIMO-MUD does not perform well

Having two antennas at the AP improves the PER performance (comparing Fig. 11(c) with Fig. 11(b)), because we have one more degree of freedom. However, the performance of conventional MIMO-MUD system does not work quite well, either. Fig. 11(c) shows the PHY-layer statistics of the MMSE decoder (since it is known that MMSE works better than ZF, we did not plot the ZF decoder's results). This is understandable because Fig. 11 is related to the balanced-power case, and MMSE is known to have degraded performance when powers from different users are balance [20].

Observation 3: MIMO-NCMA works well for QPSK

From Fig. 11(d), we can see that the number of decoded packets for both PNC and MUD decoders increase drastically for MIMO-NCMA, compared with Single-NCMA of Fig. 11(b). The reason is that we now have one more degree of freedom (e.g., the antenna space diversity). At 9dB, around 70% packets can be decoded correctly (either single packet or two packets), and at 11.5dB, the PER can be as low as less than 2%. Both PNC and MUD decoders improve after the introduction of one additional degree of freedom. Comparing Fig. 11(c) and Fig. 11(d), we can see that the MUD decoder's performance is also improved. That is, our proposed reduced-constellation MUD decoder has a better PER performance than conventional MMSE and ZF decoders for QPSK, which is consistent with the BPSK results in [1].

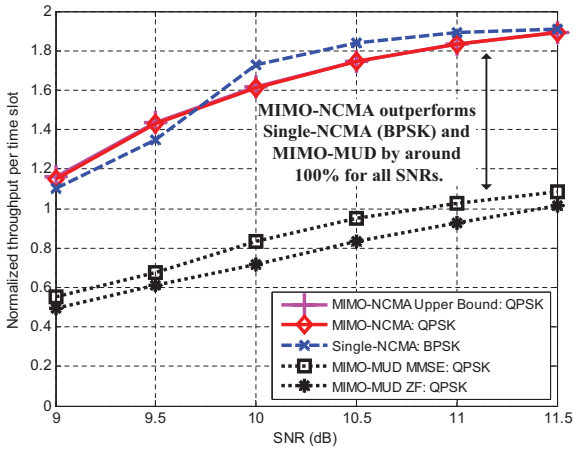


Fig. 12. MAC-layer performance: Throughput comparison of different schemes for different SNRs with $L_A = 1.5L_B = 24$.

2) MAC-layer Throughput Performance: We now evaluate the overall NCMA throughput performance at the MAC layer. In NCMA, the PHY layer could decode one or two packets in one time slot (we treat the cases of ABX, AX, BX, and AB as having two packets, and the cases of A, B, and X as having one packet). For benchmarking, we derive a theoretical upper bound for the overall MAC-layer normalized throughput imposed by the PHY-layer received data. The upper bound of NCMA is defined as

$$\text{Upper Bound} = 2 \times (\Pr\{ABX\} + \Pr\{AX|BX\} + \Pr\{AB\}) + 1 \times (\Pr\{A|B\} + \Pr\{X\}). \quad (14)$$

We note that, given the same normalized throughput, the absolute throughput of QPSK is twice that of BPSK.

We examine the MAC-layer performance by employing trace-driven simulations using the PHY-layer statistics obtained in Fig. 11. Specifically, we can obtain the probabilities of each event (i.e., ABX, AB, AX|BX, A|B and X) from the statistics. And then, we generate traces of events based on these probabilities and used these traces to drive our simulations.

Fig. 12 plots the MAC-layer throughputs of different schemes. In NCMA, the MAC-layer Reed-Solomon (RS) code constraint length parameter L (see Section II-B) can be different for different users. In this figure, L_A (L_B) is the number of packets the AP needs in order to decode M^A (M^B). We choose $L_A = 1.5L_B = 24$ based on our prior experience: the detailed explanation and justification for using asymmetric L_A and L_B can be found in [1]. The normalized throughput for NCMA systems is defined as

$$Th = \frac{L_A \times N_A + L_B \times N_B}{N_{Beacon}} \quad (15)$$

where N_A (N_B) is the number of messages of node A (B) have been recovered, and N_{Beacon} is the number of beacons. In Fig. 12, QPSK MIMO-NCMA's achievable throughput almost coincides with the theoretical upper bound. MIMO-NCMA works well with QPSK modulation, and since the absolute throughput of QPSK is twice that of BPSK, the QPSK MIMO-NCMA throughput is doubled compared with that of BPSK Single-NCMA system. In Fig. 12, we also include conventional MIMO-MUD decoders as our benchmarks. MIMO-NCMA has around 80∼100% throughput improvement over MIMO-MUD for all SNRs.

VI. Discussions

Enhanced Reduced-constellation Demodulator – In the current system, we adopt a reduced-constellation demodulation scheme for the PHY-layer PNC and MUD decoders. The soft information of I and Q bits of a QPSK symbol is calculated separately, which may potentially lead to performance degradation. An ideal reduced-constellation scheme for QPSK NCMA system should reduce the 16 constellation points to 4 directly (e.g., $1+j, 1-j, -1+j$ and $-1-j$). We will leave the exploration of the enhanced reduced-constellation demodulator as our future work.

Weighted Antenna Signal Combination – We have treated the signals from the two received antennas at the AP equally, when combining the two streams of information. The underlying assumption is that the two antennas' signals can be decoded equally well by NCMA PNC and MUD decoders. However, as is shown in Section III of this paper, different relative phase offsets may lead to different BER performance for the PHY layer decoders. A natural question (following the simple principle as maximum-ratio combining, MRC [20]) is whether weighted antenna signal combination can improve the system performance. We are currently working toward this direction.

NCMA beyond Two Users – Through experiments, we find that the lone XOR packet ratio for the two-user MIMO-NCMA system is very low (e.g., less than 10%), whereas the low XOR packet ratio for two user Single-NCMA can be as large as 20%. We conjecture that this phenomenon is due to the full degrees of freedom in our current 2×2 distributed MIMO system, where the advantage of using PNC decoder cannot be fully exploited. Things could be different if we use the two-antenna AP for the decoding of signals from more than two users. We believe that allowing more than two users to transmit together can further increase the NCMA system throughput.

VII. Conclusions

We have developed a MIMO NCMA system operated on QPSK referred to as MIMO-NCMA. MIMO-NCMA is extensible to higher-order modulations beyond QPSK. With the use of two antennas at the AP, MIMO-NCMA solves the throughput degradation problem induced by relative phase offsets between the simultaneous signals from multiple transmitters. The experiments on our software-radio MIMO-NCMA prototype show that MIMO-NCMA can double the throughput of NCMA with only one antenna at the AP. In addition, the throughput of MIMO-NCMA is above those of conventional ZF and MMSE distributed MIMO-MUD systems by 100% and 80% on average.

ACKNOWLEDGMENT

This work is supported by AoE grant E-02/08 and the General Research Funds Project Number 14204714, established under the University Grant Committee of the Hong Kong Special Administrative Region, China. This work is also supported by NSF of China (Project No. 61271277).

REFERENCES

[1] L. Lu, L. You, and S. C. Liew, "Network-coded multiple access," *IEEE Trans. Mobile Computing*, 2014.
[2] S. Zhang, S. C. Liew, and P. P. Lam, "Hot topic: physical-layer network coding," in *ACM MOBICOM*, 2006.
[3] S. Verdú, *Multiuser Detection*. Cambridge University Press, 1998.
[4] L. You, S. C. Liew, and L. Lu, "Network-coded multiple access ii : Toward realtime operation with improved performance," *IEEE Jour. Select. Areas in Comm.*, 2014.
[5] M. Wu, F. Ludwig, M. Woltering, D. Wuebben, A. Dekorsy, and S. Paul, "Analysis and implementation for physical-layer network coding with carrier frequency offset," in *Smart Antennas (WSA), 2014 18th International ITG Workshop on*. VDE, 2014, pp. 1–8.
[6] L. Lu and S. C. Liew, "Asynchronous physical-layer network coding," *IEEE Trans. Wireless Commun.*, vol. 11, no. 2, pp. 819–831, Feb. 2012.
[7] S. Long, S. C. Liew, and L. Lu, "On the subtleties of q-pam linear physical-layer network coding."
[8] S. Liew, S. Zhang, and L. Lu, "Physical-layer network coding: Tutorial, survey, and beyond," *Physical Communication*, vol. 6, no. 1, pp. 4–42, 2013.
[9] B. Nazer and M. Gastpar, "Reliable physical layer network coding," *Proceedings of the IEEE*, vol. 99, no. 3, pp. 438–460, 2011.
[10] L. Lu, T. Wang, S. Liew, and S. Zhang, "Implementation of physical-layer network coding," *Physical Communication*, vol. 6, no. 1, pp. 74–87, 2013.
[11] L. Lu, L. You, Q. Yang, T. Wang, M. Zhang, S. Zhang, and S. C. Liew, "Real-time implementation of physical-layer network coding," in *ACM SRIF*, 2013, pp. 71–76.
[12] G. Cocco, C. Ibars, D. Gunduz, and O. del Rio Herrero, "Collision resolution in slotted aloha with multi-user physical-layer network coding," in *Vehicular Technology Conference (VTC Spring), IEEE 73rd, 1-4*, 2011.
[13] G. Cocco and S. Pfletschinger, "Seek and decode: Random multiple access with multiuser detection and physical-layer network coding," in *Communications Workshops (ICC), IEEE International Conference on, 501-506*, 2014.
[14] G. Liva, "Graph-based analysis and optimization of contention resolution diversity slotted aloha," *IEEE Trans. on Comm., vol. 59, no. 2, pp. 477–487*, Feb. 2011.
[15] A. Gudipati and S. Katti, "Strider: Automatic rate adaptation and collision handling," in *ACM SIGCOMM*, 2011.
[16] A. Gudipati, S. Pereira, and S. Katti, "AutoMAC: rateless wireless concurrent medium access," in *ACM MOBICOM*, 2012.
[17] K. Tan, H. Liu, J. Fang, W. Wang, J. Zhang, M. Chen, and G. M. Voelker, "Sam: Enabling practical spatial multiple access in wireless lan," in *ACM MOBICOM*, 2009.
[18] H. S. Rahul, S. Kumar, and D. Katabi, "JMB: scaling wireless capacity with user demands," in *ACM SIGCOMM*, 2012.
[19] H. V. Balan, R. Rogalin, A. Michaloliakos, K. Psounis, and G. Caire, "AirSync: Enabling distributed multiuser MIMO with full spatial multiplexing," *IEEE/ACM Transactions on Networking*, vol. 6, no. 21, pp. 1681–1695, 2013.
[20] D. Tse and P. Viswanath, *Fundamentals of wireless communication*. Cambridge university press, 2005.
[21] D. Halperin, W. Hu, A. Sheth, and D. Wetherall, "Predictable 802.11 packet delivery from wireless channel measurements," in *ACM SIGCOMM*, 2010.
[22] IEEE 802.11-2009, "Wireless LAN medium access control (MAC) and physical layer (PHY) specifications amendment 5: Enhancements for higher throughput."
[23] IEEE802.11ac-2013, "Wireless LAN medium access control (MAC) and physical layer (PHY) specifications amendment 4: Enhancements for very high throughput for operation in bands below 6 GHz."
[24] Ettus Inc., "Universal software radio peripheral."